



## Impact of modified turbulent diffusion of PM<sub>2.5</sub> aerosol in WRF-Chem simulations in Eastern China

Wenxing Jia<sup>1,2</sup>, Xiaoye Zhang<sup>2,3\*</sup>

<sup>1</sup>Key Laboratory for Aerosol-Cloud-Precipitation of China Meteorological Administration, Nanjing  
5 University of Information Science & Technology, Nanjing, 210044, China

<sup>2</sup>Key Laboratory of Atmospheric Chemistry of CMA, Chinese Academy of Meteorological Sciences,  
Beijing, 100081, China

<sup>3</sup>Center for Excellence in Regional Atmospheric Environment, IUE, Chinese Academy of Sciences,  
Xiamen, 361021, China

10 Correspondence to: X. Zhang ([xiaoye@cma.gov.cn](mailto:xiaoye@cma.gov.cn))

### Abstract

Correct description of the boundary layer mixing process of particle is an important prerequisite to understanding the mechanism of heavy pollution episodes. Turbulent mixing process of particles is usually denoted by the turbulent diffusion relationship of heat, meaning that the turbulent transport of particles and heat are similar. This similarity has, however, never been verified. Here we investigate the dissimilarity between particles and heat, indicating that the unified treatment of all scalars in the model is questionable. Using mixing-length theory, the turbulent diffusion relationship of particle is established, embedded in the model and verified on a long-term scale. Simulated results of PM<sub>2.5</sub> concentration were improved by 8.3% (2013), 17% (2014), 11% (2015) and 11.7% (2017) in Eastern China, respectively. However, under the influence of complex topography, the turbulent diffusion process is insensitive to the simulation of the pollutant concentration. In addition to the PM<sub>2.5</sub> concentration, the simulation of the CO concentration has also been improved, which shows that the turbulent diffusion process is extremely critical to the change in the concentration of pollutants.



## 1 Introduction

25 Along with the intensive urbanization and tremendous economic development, numerous incidents of aerosol pollution have frequently occurred in China (An et al., 2019; Q. Zhang et al., 2019; X. Zhang et al., 2019). Aerosol pollution, characterized by  $PM_{2.5}$ , occurs primarily in the planetary boundary layer (PBL). The horizontal transportation and vertical distribution of pollutants are obviously affected by the PBL mixing process, associated with intricate turbulence eddies (Liu et al., 2018; Ren et al., 2018; Wang et al., 2018; Du et al., 2020). Turbulent transport, as a vital process, controls the exchange of momentum, heat, water vapor and pollutants through turbulence eddies within the PBL (Stull, 1988).

Turbulent transports of temperature, water vapor and  $CO_2$  has long been considered similar (Kays et al., 2005). However, this statement is usually invalid and is regarded as applicable only under neutral stratifications. Previous researchers have demonstrated that temperature-humidity dissimilarity, and such a disparity between the effectiveness of heat and water vapor transport, is due to different mechanisms of scalar transport (Katul et al., 2008; van de Boer et al., 2014; Guo et al., 2020). For example, the effect of advection (Assouline et al., 2008), entrainment at the top of PBL (Cava et al., 2008; Gao et al., 2018) and heterogeneity in sources and sinks (Detto et al., 2008; Wang et al., 2014; Guo et al., 2016). Moriwaki and Kanda (2006) also indicated that the differences of turbulent transport between heat and  $CO_2$  were due to both by the active role of temperature and the heterogeneity of the source distribution. Li and Bou-Zeid (2011) revealed that the transport dissimilarity between the momentum and the scalar likely resulted from the topology of turbulent structures. As a result, there are differences between turbulent transport of vectors and scalars, or between scalars. However, less attention has been paid to turbulent transport of particles. Dupont et al. (2019) have proven that the turbulent dissimilarity of transport between dust, heat and momentum. The only studies assumed that particles were considered passive scalars with the same source/sink as heat, and that they used similarity to correct particle flux from the heat flux (Damay et al., 2009; Deventer, Held et al., 2015). A key question is whether the turbulent transport between temperature and particles is similar. This similarity has, however, never been verified, due to the lack of observational turbulence data of particles.



50 The turbulent diffusion processes of all scalars (including active and passive scalars) are dealt with in a unified manner in the current model. To date, only a few studies have shown that pointed out the meteorological fields and pollutants can be changed by adjusting the minimum value of turbulent diffusion coefficient (TDC) (Savijarvi et al., 2002; Wang et al., 2018; Du et al., 2020; Liu et al., 2021), increasing turbulent kinetic energy (TKE) (Foreman and Emeis, 2012) and modifying experiment  
55 expressions (Sušelj and Sood, 2010; Huang and Peng, 2017). Recently, Jia et al. (2021) obtained the TDC of particles by using high-resolution vertical flux data of particles based on the mixing length theory. Additionally, this relationship has been embedded into the WRF-Chem model to calculate the PBL mixing process of pollutants separately. This work has initially improved the overestimation of pollutant concentration at night in winter 2016 in Eastern China. However, a series of heavy pollution incidents  
60 have occurred and attracted much attention since 2013 (Yang et al., 2018; Zhong et al., 2019). Therefore, we conducted a series of simulations for the heavy pollution periods in winter from 2013 to 2017 in this study. The difference between this study and previous work is that previous work focused on the analysis of observations, while this study mainly explores the uncertainty of the influence of the model on the turbulent diffusion of particles.

## 65 **2 Data and methods**

### **2.1 Data**

In this study, the aerosol pollution level is denoted by the hourly surface  $PM_{2.5}$  concentration that is available from the official website of the China National Environmental Monitoring Center from 1 January 2013 to 31 January 2017.  $PM_{2.5}$  concentration stations increased from 35 cities in  
70 2013(illustrated by red dots in Fig. 1b) to 78 cities in 2017(illustrated by black dots in Fig. 1b) in Eastern China. In addition to  $PM_{2.5}$  observations, the hourly concentrations of CO were acquired from the National Air Quality real-time publication platform (<http://106.37.208.233:20035>, last access: 20 May 2021). Aside from this, the hourly meteorological observation data, including temperature, pressure, relative humidity, wind and visibility from the national automatic weather stations (AWS) provided by  
75 the National Meteorological Information Center of China Meteorological Administration (NMICMA) (illustrated by gray crosses in Fig. 1b). The time period of the data selected is from 1 January 2013 to 31



January 2017. In addition, observational turbulence data are obtained from the Pingyuan County Meteorological Bureau (37.15°N, 116.47°E), Shandong Province, from 27 December 2018 to 8 January 2019 (illustrated by orange triangle in Fig. 1b). Identical eddy-covariance systems were operated, including three-dimensional sonic anemometer-thermometer (IRGASON, Campbell Scientific, USA) and CO<sub>2</sub>/H<sub>2</sub>O open-path gas analyzer (LI7500, LI-COR, USA). These instruments measured three components of wind speed, potential temperature, water vapor and CO<sub>2</sub> concentrations with a frequency of 10 Hz. The turbulence data finally was split into 30-min segments. In addition, a continuous particle measuring instrument E-sampler () and a high-frequency sampling visibility sensor CS120A () were used to obtain PM<sub>2.5</sub> mass concentration every minute and visibility of 1 Hz. The calculation of 30-min vertical flux of PM<sub>2.5</sub> is based on the nonlinear relationship between PM<sub>2.5</sub> concentration and visibility (Ren et al., 2020). Detailed background and calculation principle of this method were presented in Ren et al. (2020), so we only describe key steps. Firstly, we separate PM<sub>2.5</sub> concentration ( $C$ ) and visibility datasets ( $V$ ) into mean and turbulent deviations (i.e.,  $c = \bar{c} + c'$  and  $V = \bar{V} + V'$ ). Secondly, we get the fitted coefficients by using exponential correlation between the PM<sub>2.5</sub> concentration and visibility (i.e.,  $c = a \cdot V^b$ ). Thirdly, combining the first two steps, we can get the turbulent fluctuations of PM<sub>2.5</sub> concentration (i.e.,  $c' = a \cdot (\bar{V} + V')^b - \bar{c}$ ). Finally, we use fluctuations of vertical velocity (i.e.,  $w'$ ) and of PM<sub>2.5</sub> concentration (i.e.,  $c'$ ) to calculate the vertical flux of PM<sub>2.5</sub> (i.e.,  $\overline{w'c'}$ ).

To investigate the influence of the PBL height (PBLH) on the PM<sub>2.5</sub> pollution, soundings collected at the Fuyang site (32.54°N, 115.5°E) and the Anqing site (30.37°N, 116.58°E) (illustrated by yellow pluses in Fig. 1b) for the period 2013-2017 were analyzed. These two stations are equipped with L-band radiosonde systems (Miao et al., 2018), which proved a fine resolution (1 Hz) profiles of temperature, relative humidity and wind speed two times (0800 and 2000 BJT) a day during winter. To eliminate the error caused by the difference of calculation methods of PBLH, Richardson number method is used to calculate the PBLH in both observation and simulation. The Richardson number is defined as follows:

$$Ri(z) = \frac{g(\theta_{vs} - \theta_z)(z - z_s)}{\theta_{vs} (u_z - u_s)^2 + (v_z - v_s)^2} \quad (1)$$



where  $z$  is the height above ground,  $g$  is the gravity,  $\theta_s$  is the virtual potential temperature, and  $u$  and  $v$  are the component of wind. The subscript “s” denotes the surface level. The height at which the Richardson number equals 0.25 is defined as the PBLH.

## 105 2.2 Numerical simulation

Long-term three-dimensional simulation experiments are enforced in this study from the winter of 2013 to 2017, when Eastern China frequently experienced severe and persistent aerosol pollution events (Zhong et al., 2019). One month for each winter from 2013 to 2017 was selected, and a total of four months were confirmed, which are January 2013, December 2014, December 2015 and January 2017, respectively. The anthropogenic emissions of BC, OC, CO, NH<sub>3</sub>, NO<sub>x</sub>, PM<sub>2.5</sub>, PM<sub>10</sub> and volatile organic compounds (VOCs) are set based on the monthly Multi-resolution Emission Inventory for China (MEIC) from 2013 to 2017 are provided by Tsinghua University, with a resolution of 0.25°×0.25° (<http://meicmodel.org/>, last access: 20 May 2021). The model domain was centered over Eastern China with a horizontal resolution of 33 and 6.6 km (Fig. 1a). The model top was set to the 50 hPa level, and 48 vertical layers were configured below the top. To resolve the PBL structure, 21 layers below 2 km (AGL) were set. The physics parameterization schemes selected for this study included the Morrison double-moment microphysics scheme (Morrison et al., 2009), RRTMG longwave/shortwave radiation schemes (Iacono et al., 2008), MM5 similarity surface layer scheme (Jiménez et al., 2012), Noah land surface scheme (Chen and Dudhia, 2001), Singer-layer UCM scheme (Kusaka et al., 2001), CLM4.5 lake physics scheme (Subin et al., 2012; Gu et al., 2015), ACM2 planetary boundary layer scheme (Pleim, 2007), Grell-3D cumulus scheme (Grell and Devenyi, 2002). And the chemical mechanism is the RADM2-MADE/SORGM scheme (Ackermann et al., 1998; Schell et al., 2001). The initial and boundary conditions of meteorological fields were set up using the National Centers for Environmental Prediction (NCEP) global final (FNL) reanalysis data, with a resolution of 1° × 1° (<https://rda.ucar.edu/datasets/ds083.2/>, last access: 20 May 2021). And the initial and boundary conditions of chemical fields were configured using the global model output of Model for Ozone and



Related Chemical Tracers (MOZART) (<http://www.acom.ucar.edu/wrf-chem/mozart.shtml>, last access: 20 May 2021).

Simulation using abovementioned configurations is referred to as the original runs. In the original PBL  
130 parameterization scheme, TDCs of heat and momentum are different (i.e.,  $K_h \neq K_m$ ), the turbulent mixing  
process of pollutants is similar to that of heat, which supposes the eddy diffusions of particles and heat  
are identical (i.e.,  $K_h = K_c$ ). While in the improved scheme, the eddy diffusion of particles is calculated by  
the TDC of particles (i.e.,  $K_c$ ), which is different from that of heat (i.e.,  $K_c \neq K_h$ ). These improved  
experiments are regarded as the new runs hereafter. All simulation included a total of eight months. The  
135 91-h simulation is conducted beginning from 0000UTC of three days ago for each day (i.e., 248  
simulation experiments), and first 64-h of each simulation is considered as the spin-up period.

The TDC is parameterized by the mixing length ( $l$ ) and the function of Richardson number ( $f(Ri)$ ), that  
is

$$K = 0.01 + \sqrt{ss} \cdot l^2 \cdot f(Ri) \quad (2)$$

where  $ss$  is the wind shear (i.e.,  $ss = (\partial u / \partial z)^2 + (\partial v / \partial z)^2$ ), 0.01 refers to the minimum value of TDC  
140 in the model, and the mixing length formula (i.e.,  $l = \kappa z / (1 + \kappa z / \lambda)$ ,  $\lambda = 80$ ) proposed by Blackadar  
(1962) is widely used in the model (Louis, 1979; Liu and Carroll, 1996; Lin et al., 2008; Pleim, 2016).  
Many previous studies have showed various functions of Richardson number, which represent the  
different situations of turbulence.

(i) For the stable conditions (i.e.,  $Ri \geq 0$ ), Esau and Byrkjedal (2007) suggested:

$$f_h = (1 + 10Ri + 50Ri^2 + 5000Ri^4)^{-1} + 0.0012 \quad (3)$$

$$f_m = 0.8f_h + 0.00104 \quad (4)$$

145 where  $f_h$  and  $f_m$  denote the function of heat and momentum, respectively, and these functions have been  
implemented in the model. We added an additional function of particles into the model, that is



$$f_c = (1 + 66.6Ri)^{-1} \quad (5)$$

which is used to denote the turbulent mixing process of particles within the PBL. For detailed analysis and comparison of functions, please refer to Jia et al. (2021).

(ii) For the unstable conditions ( $Ri < 0$ ), Equation (2) is rewritten as:

$$K_h = 0.01 + \sqrt{ss \cdot (1 - 25Ri)} \cdot l^2 \quad (6)$$

$$K_m = 0.8 \cdot K_h \quad (7)$$

150 Considering that the pollution is usually accompanied by the stable boundary layer, we mainly modify the program of the stable boundary layer, while for the unstable boundary layer, we still use the default program of the original scheme.

There are several important things to note about the TDC of particles. (1) It is calculated by the explicit local gradient to represent the PBL mixing process of particles, which are more suitable in the stable  
155 boundary layer (SBL). (2) The new scheme avoids the inapplicability of the Monin-Obukhov similarity theory (MOST), the deviation of the PBLH in the SBL, higher computational efficiency (Li et al., 2010), and it is easier to apply to forecasting models in the future. (3) It is used to evaluate the PBL mixing process of pollutants separately, which can improve the simulation results of pollutants and does not deteriorate the simulation results of meteorological parameters.

### 160 **3 Temperature-particles transport dissimilarity**

The  $PM_{2.5}$  concentration frequently reached hazardous levels above  $100 \mu\text{g m}^{-3}$  during six heavy pollution episodes (marked by HPE1-HPE6 in Fig. S1). The turbulent characteristics of  $PM_{2.5}$  concentration have been demonstrated in Ren et al. (2020), and the turbulence characteristics of heat and particles were markedly different (Jia et al., 2021; Ren et al., 2021). Based on the previous studies, the turbulent  
165 correlation coefficient is used to evaluate the transport efficiencies for heat, water vapor, momentum and particles (Stull, 1988; Li and Bou-Zeid, 2011; Dupont and Patton, 2012). The expression as follows:



$$R_{wp} = \frac{\overline{w'p'}}{\sigma_w \sigma_p} \quad (8)$$

$R_{wp}$  denotes the correlation coefficient between the fluctuations of  $w'$  and  $p'$ , while  $p$  stands for the temperature  $T$ , specific humidity  $q$ , longitudinal velocity component  $u$  and particles  $c$ . This value is between -1 to 1 (negative correlation to positive correlation), and zero indicates that the two parameters are uncorrelated. The  $\sigma_w$  and  $\sigma_p$  are the standard deviations of vertical velocity and parameter  $p$  (i.e.,  $T$ ,  $q$ ,  $u$ ,  $c$ ) over a 30-min interval, respectively. If the MOST is applicable, it indicates the turbulent mechanisms of heat, water vapor and particles are the same, i.e.,  $R_{wt}=R_{wq}=R_{wc}$  (Liu et al., 2017). Previous studies have investigated different mechanisms of scalar transport between temperature and humidity (Moriwaki and Kanda 2006; Katul et al., 2008; van de Boer et al., 2014; Guo et al., 2016, 2020). Lacking profile data for the  $PM_{2.5}$  concentration (Yuan et al., 2019; Ren et al., 2020), there is little about the transport efficiency of fine particles (i.e.,  $PM_{2.5}$ ). The correlation coefficient of heat flux and particle flux can be defined as:

$$R_{wt,wc} = \frac{\overline{(w't' - \overline{w't'}) (w'c' - \overline{w'c'})}}{\sigma_{w't'} \sigma_{w'c'}} \quad (9)$$

$\sigma_{w't'}$  and  $\sigma_{w'c'}$  are the standard deviations of  $w't'$  and  $w'c'$ , respectively. The correlation coefficients of the heat ( $R_{wt}$ ), fine particles ( $R_{wc}$ ), and heat flux and particle flux ( $R_{wt,wc}$ ) are presented in Fig. 2. Clearly, there is an obvious difference between  $R_{wt}$  and  $R_{wc}$ . Whether transport efficiency is  $R_{wt}$  or  $R_{wc}$ , transport efficiency can exhibit the greatest variability at night during the HPEs, probably suggesting an increasing complexity of turbulent structures at night (Fig. 2b and 2c). High correlation exists between heat and fine particles fluxes at night (especially at the wee hours) in the HPEs (Fig. 2d), which indicates that these fluxes are performed by the same motions within the PBL. Previous research has noted that the atmospheric vertical mixing is mainly controlled by the large-scale eddies' percentage at night during the HPEs (Li et al., 2020). However, it should be mentioned that the correlation coefficient between heat and fine particles fluxes ( $R_{wt,wc}$ ) changes dramatically at night (Fig. 2d). This means that these two fluxes transported with different eddies in a short time, or transported at different time periods by the same eddy when the correlations diminish. Consequently, there is a difference between the transport of heat and fine



190 particles fluxes. Whether scalar is temperature or particle, it is debatable that the mixing process of all  
scalars are dealt with a unified manner within the PBL. As a result, we urgently need to develop a TDC  
of particles, which is used only to calculate the mixing process of pollutants within the PBL.

#### 4 Improvement of PM<sub>2.5</sub> concentration

Based on the TDC relationship of particles in the previous study (Jia et al., 2021), this study applies this  
195 relationship to a long-term scale simulation for verification. Figure 3 shows the average value of  
simulated and observed PM<sub>2.5</sub> concentration at night from 2013 to 2017, and the PM<sub>2.5</sub> concentration was  
overestimated to varying degrees in Eastern China. The relative bias (RB) in the mean regional value is  
as high as 11.8% (2013), 48% (2014), 23.8% (2015) and 20.9% (2017), respectively (Fig. 3i-l).  
Compared to the original scheme, the new scheme improves the situation where the pollutant  
200 concentration is overestimated at night in Eastern China (Fig. 4a-d). The degree of overestimation of the  
pollutant concentration is reduced, and the relative bias of average value of the new scheme is 3.5%  
(2013), 31% (2014), 12.8% (2015) and 9.2% (2017), respectively (Fig. 4e-h). Moreover, the absolute  
bias in the mean value is reduced by 8.3% (2013), 17% (2014), 11% (2015) and 11.7% (2017),  
respectively (Fig. 4i-l). To better evaluate the model performance, figure 5 shows the Taylor diagram of  
205 hourly PM<sub>2.5</sub> concentration, and the black (red) dots indicate original (new) simulation results at all  
stations from 2013 to 2017. The statistical results present a consistent feature, that is, the worse the  
simulation results of the original scheme are, the more obvious improvement of the new scheme becomes  
(arrows indicate improved stations in the Fig. 5). The results indicate that the pollutant concentrations at  
all stations are not improved to the same extent. When the original scheme overestimates the pollutant  
210 concentrations, the new scheme will reduce the degree of overestimation. While the pollutant  
concentrations are underestimated by the original scheme, the new scheme does not increase the degree  
of underestimation again (Fig. 5). And the standard deviation (normalized) of the mean value is decreased  
by 0.2 (2013), 0.28 (2014), 0.14 (2015) and 0.16 (2017) (Fig. 5). As a whole, the new scheme can  
significantly improve the common phenomenon of overestimated pollutant concentration in the SBL in  
215 Eastern China (Fig. 5).



In addition to the changes in the pollutant concentration near the surface, we should also pay attention to the changes in the pollutant concentration in the vertical direction. Theoretically, increasing turbulent diffusion will reduce the pollutant concentrations near the surface-layer, and the pollutants will be more fully mixing in the vertical direction, which results in lower concentrations of pollutants in the near surface-layer and higher concentrations of pollutants in the upper layer. Actually, the pollutant concentration is reduced in the surface-layer and it is increased in the upper layer at night (Fig. 6), which is consistent with the theory.

## 5 Uncertainty analysis

### 5.1 Meteorological parameters

Depending on the transport dissimilarity of heat and particles, the TDC of particles was added separately in the model to calculate the turbulent mixing process of particles. For correctional approaches, it is important that a new scheme does not lead to worse performance than that with the original scheme. To verify the new scheme without affecting the simulation results of the meteorological parameters, the simulation results of the near-surface meteorological elements (i.e., 2-m temperature, 2-m relative humidity and 10-m wind speed) have been compared and analyzed. It can be seen from Figure S2-S4 that the correlation coefficients of meteorological parameters by two schemes are greater than 0.99, noting that the new scheme does not alter the performance of meteorological fields, which is an advantage of the new scheme. Compared with previous studies, modifying the turbulent diffusion coefficient of heat not only affects the simulation of temperature (Savijarvi and Kauhanen, 2002), but also influences the results of pollutants (Liu et al., 2021). Improving the parameterization scheme is a long and tough process, making it difficult to improve the simulation results of all parameters at once. When the simulation results of one parameter are improved, we should first seek to ensure that the simulation results of other parameters are not deteriorated. Then, we are going to look at improving other parameters. Although the aerosol-radiation two-way feedback process has been considered in the atmospheric-chemistry two-way coupled model, the mean fractional change in  $PM_{2.5}$  concentration varying just a few percent (Li et al., 2017; Wu et al., 2019; Gao et al., 2020). We should focus more on the feedback process between turbulence and aerosol, and hopefully develop a turbulence-aerosol two-way feedback module.



Some turbulent characteristics (e.g., turbulence barrier effect) can be taken into consideration during the HPEs, reflecting a more realistic pollutant concentration evolution process. We think the next step is to  
245 solve this major problem.

## 5.2 PBL height

Although PBL height (PBLH) is widely used to determine the effective air volume and atmospheric environmental capacity for pollutant diffusion (Miao et al., 2018), the influence of PBLH on the pollution is uncertain. (1) There are various methods to determine the PBLH, either through observation or  
250 simulation (Jia and Zhang., 2020; Zhang et al., 2020). Various methods diagnose different PBLH, which reinforces uncertainty about the PBLH as a criterion. (2) There does not necessarily reflect a negative correlation between pollutant concentration and PBLH. The relationship between the PBLH and  $PM_{2.5}$  pollution has been revealed on the basis of the four-year radiosonde measurements, and the results show that the correlation between PBLH and  $PM_{2.5}$  concentration is different in various regions (Miao et al.,  
255 2018). Moreover, when the PBLH is higher, the corresponding pollutant concentration is not necessarily lower (Miao et al., 2021). When there is a transport stage during the HPEs with a high wind speed, the mechanical turbulence is strong, and the PBLH and pollutant concentration increase simultaneously. Therefore, the relationship between PBLH and  $PM_{2.5}$  pollution is intricate. The impact of PBLH is ultimately represented through the TDC in the model, because the PBLH is used to calculate TDC. If the  
260 pollutant concentration is clearly controlled by the PBLH, when the pollutant concentration is overestimated and the PBLH is to be underestimated. However, the PBLH is reproduced well by the model, and the model does not underestimate the PBLH (Fig. 7). The new scheme does not disturb the simulation results of meteorological fields, and therefore does not affect the simulation results of PBLH (Fig. S5). The results of the simulation of pollutant concentration are improved under the similar PBLH,  
265 which further demonstrates that the simulation of pollutant concentration is not only controlled by the PBLH.



### 5.3 Influence of other processes

Overestimating of pollutant concentrations has been improved in Eastern China, but there are also some sites in northern China where pollutant concentrations are underestimated. These sites (i.e., Hebei and Beijing) are mostly located in the east of the Taihang Mountains and the south of the Yan Mountains (Fig. 8). For example, in December 2016, the pollutant concentrations of all sites in Beijing were not underestimated. Jia et al. (2021) have found that the pollutant concentrations of two sites located in the south of Beijing (i.e., blue dots in Fig. S2 in Jia et al., 2021) are well reproduced by the model (i.e., away from the mountain). This phenomenon also occurred in 2013-2017 (Fig. 8), and the pollutant concentrations were significantly underestimated at some sites (i.e., near the mountain). The boundaries of overestimated and underestimated sites are pronounced in Beijing-Tianjin-Hebei region (white dashed in Fig. 8), and the pollutant concentration is overestimated at some sites, which are away from the mountain (i.e., Tianjin and southeast of Hebei). Furthermore, we found that the TDC of particles in the new scheme is significantly smaller than the TDC of heat in the original scheme in the mountain area (red rectangle in Fig. S6). The terrain will disturb the turbulence fields, making the stable stratification weakly stable/unstable. Theoretically, the reduced TDC will increase the pollutant concentration near the mountain, and improve the underestimation of pollutant concentration of the original scheme. However, the change of TDC does not improve the underestimation of pollutant concentration in the mountain area, which shows that the impact of other processes is more obvious in the mountain area. For instance, the advection process is strongly related to the wind and pollutant concentration gradients from upwind areas to downwind areas (Gao et al., 2018). Figure S7 shows that the wind speed is much more overestimated in the mountain areas (two purple rectangles in Fig. S7i-l), but only the pollutant concentration is always underestimated in the BTH region (Fig. 3i-l). Clear gradients of wind speed and pollutant concentration exist in the BTH region (Fig. 3a-d; Fig. S7a-d), so these sites (i.e., closer to the mountain) may be significantly affected by the advection process. Hence, the influences of other processes or topography in the mountain area deserve further consideration in the future.

Whether the simulation of chemical components has been improved, it cannot be well verified because of the lack of observational data. Although the observational components of PM<sub>2.5</sub> are not available to evaluate the simulation results of new scheme, CO, as a representative of primary pollutants, can be



295 compared to the observations. Results from new scheme with TDC of particles are more consistent with  
the observations than the original scheme (Fig. S8), which supports the improvement of  $PM_{2.5}$   
concentration (Fig. 5 and S8).

## 6 Conclusions and prospects

Mesoscale model faces numerous challenges during the heavy pollution events. One of these challenges  
300 is the correct description of the turbulent mixing of pollutants. Although the model can reproduce the  
evolution of pollutants, the simulation of the diurnal variation of pollutants is fundamentally flawed,  
especially at night. Errors in estimation of pollutant concentration are primarily caused by defects in the  
turbulent mixing of pollutants in the model. Actually, there is a difference between the turbulent transport  
of heat and particles. This result inspires us to deal with the turbulent diffusion of heat and particles  
305 separately. Therefore, based on the turbulent diffusion expression of particles proposed by Jia et al., 2021,  
we again audited the improvement of pollutant concentration in winter from 2013 to 2017.

The original scheme overestimates the surface  $PM_{2.5}$  concentration by 11.8% (2013), 48% (2014), 23.8%  
(2015) and 20.9% (2017) at night, respectively. The new scheme has improved the overestimation of the  
surface  $PM_{2.5}$  concentration in eastern China at night, and the average absolute bias of average value can  
310 be reduced by 8.3% (2013), 17% (2014), 11% (2015) and 11.7% (2017), respectively. In the vertical  
direction, the pollutant concentration is decreased in the surface-layer while it increased in the upper  
layer. Moreover, the improvement of the pollutant concentration field does not interfere with changing  
meteorological fields. Although the PBLH affects the diffusion of pollutants, the simulation of pollutant  
concentration is not specifically controlled by the PBLH, but by TDC. However, TDC has a negligible  
315 impact on the simulation of pollutant concentration at some sites with complex topography.  $PM_{2.5}$   
components cannot be used to evaluate the results of the simulation of the new scheme, due to the lack  
of observational data. CO, however, as a representative of primary pollutants, can be compared to  
observations. Results from new scheme are more consistent with the observations than the original  
scheme, which supports the improvement of  $PM_{2.5}$  concentration. The new scheme could provide  
320 promising guidance during the heavy pollution events. The turbulent transport mechanism and scalar  
parameterization is a complex topic (Smedman et al., 2007, Lemon et al., 2019; Couvreux et al., 2020;



Edwards et al., 2020), and beyond that, other processes also need in-depth understanding and exploration (Seinfeld et al., 2016; Shao et al., 2019; Emerson et al., 2020). Therefore, more research during the heavy pollution events, especially on the experimental side (e.g., extensive measurement campaigns), might  
325 shed more light on the turbulent mixing process of pollutants and their mechanisms.

### Data availability

The surface PM<sub>2.5</sub> concentration, meteorological data, turbulent datasets and turbulent flux data of PM<sub>2.5</sub> are available by request (xiaoye@cma.gov.cn).

### Author contributions

330 Development of the ideas and concepts behind this work was performed by all the authors. Model execution, data analysis and paper preparation were performed by WJ and XZ with feedback and advice.

### Competing interests

The authors declare that they have no conflict of interest.

### Acknowledgments

335 The authors would like to acknowledge the Tsinghua University for the support of emission data.

### Financial support

This research is supported by the NSFC Project (U19A2044); National Key Project of MOST (2016YFC0203306); Atmospheric Pollution Control of the Prime Minister Fund (DQGG0104); Key Projects of Fundamental Scientific Research Fund of CAMS (2017Z001).

### 340 References

- Ackermann, I. J., Hass, H., Memmesheimer, M., Ebel, A., Binkowski, F. S., and Shankar, U.: Modal aerosol dynamics model for Europe, *Atmos. Environ.*, 32, 2981–2999, [https://doi.org/10.1016/S1352-2310\(98\)00006-5](https://doi.org/10.1016/S1352-2310(98)00006-5), 1998.
- An, Z., Huang, R., Zhang, R., Tie, X., Li, G., Cao, J., Zhou, W., Shi, Z., Han, Y., Gu, Z., and Ji, Y.: Severe  
345 haze in northern China: A synergy of anthropogenic emissions and atmospheric processes, *P. Natl. Acad. Sci. USA*, 116, 8657–8666, <https://doi.org/10.1073/pnas.1900125116>, 2019.
- Assouline, S., Tyler, S. W., Tanny, J., Cohen, S., Bou-Zeid, E., Parlange, M. B., and Katul, G. G.: Evaporation from three water bodies of different sizes and climates: measurements and scaling analysis, *Adv. Water Resour.*, 31, 160–172, <https://doi.org/10.1016/j.advwatres.2007.07.003>, 2008.



- 350 Blackadar, A. K.: The vertical distribution of wind and turbulent exchange in a neutral atmosphere, *J. Geophys. Res.*, 67, 3095–3102, <https://doi.org/10.1029/JZ067i008p03095>, 1962.
- Cava, D., Katul, G. G., Sempreviva, A. M., Giostra, U., and Scrimieri, A.: On the anomalous behaviour of scalar flux-variance similarity functions within the canopy sub-layer of a dense alpine forest, *Bound.-Lay. Meteorol.*, 128, 33–57, <https://doi.org/10.1007/s10546-008-9276-z>, 2008.
- 355 Chen, F., and Dudhia, J.: Coupling an advanced land surface – hydrology model with the Penn State – NCAR MM5 modeling system. Part I: model implementation and sensitivity, *Mon. Weather Rev.*, 129, 569–585, [https://doi.org/10.1175/1520-0493\(2001\)129<0587:CAALSH>2.0.CO;2](https://doi.org/10.1175/1520-0493(2001)129<0587:CAALSH>2.0.CO;2), 2001.
- Couvreux, F., Bazile, E., Rodier, Q., Maronga, B., Matheou, G., and Chinita, M. J., Edwards, J., Stratum, B. J. H., van Heerwaarden, C. C., Huang, J., Moene, A. F., Cheng, A., Fuka, V., Basu, S., Bou-Zeid, E., Canut, G., and Vignon, E.: Intercomparison of large-eddy simulations of the Antarctic boundary layer for very stable stratification, *Bound.-Lay. Meteorol.*, 176, 369–400, <https://doi.org/10.1007/s10546-020-00539-4>, 2020.
- 360 Damay, P. E., Maro, D., Coppalle, A., Lamaud, E., Connan, O., Hébert, D., Tallbaut, M., and Irvine, M.: Size-resolved eddy covariance measurements of fine particle vertical fluxes, *J. Aerosol Sci.*, 40, 1050–1058, <https://doi.org/10.1016/j.jaerosci.2009.09.010>, 2009.
- 365 Detto, M., Katul, G., Mancini, M., Montaldo, N., and Albertson, J. D.: Surface heterogeneity and its signature in higher-order scalar similarity relationships, *Agric. For. Meteorol.*, 148, 902–916, <https://doi.org/10.1016/j.agrformet.2007.12.008>, 2008.
- Deventer, M. J., El-Madany, T., Griessbaum, F., and Klemm, O.: One-year measurement of size-resolved particle fluxes in an urban area, *Tellus B: Chem. Phys. Meteorol.*, 67, 25531, <https://doi.org/10.3402/tellusb.v67.25531>, 2015.
- 370 Du, Q., Zhao, C., Zhang, M., Dong, X., Cheng, Y., Liu, Z., Hu, Z., Zhang, Q., Li, Y., Yuan, R., and Miao, S.: Modeling diurnal variation of surface PM<sub>2.5</sub> concentrations over East China with WRF-Chem: impacts from boundary-layer mixing and anthropogenic emission, *Atmos. Chem. Phys.*, 20, 2839–2863, <https://doi.org/10.5194/acp-20-2839-2020>, 2020.
- 375 Dupont, S., and Patton, E. G.: Momentum and scalar transport within a vegetation canopy following atmospheric stability and seasonal canopy changes: The CHATS experiment, *Atmos. Chem. Phys.*, 12, 5913–5935, <https://doi.org/10.5194/acp-12-5913-2012>, 2012.



- Dupont, S., Rajot, J.-L., Labiadh, M., Bergametti, G., Lamaud, E., Irvine, M. R., Alfaro, S. C., Bouet, C.,  
380 Fernandes, R., Khalfallah, B., Marticorena, B., Bonnefond, J. M., Chevaillier, S., Garrigou, D.,  
Henry-des-Tureaux, T., Sekrafi, S., and Zapf, P.: Dissimilarity between dust, heat and momentum  
turbulent transports during Aeolian soil erosion, *J. Geophys. Res.-Atmos.*, 124, 1064–1089,  
<https://doi.org/10.1029/2018JD029048>, 2019.
- Edwards, J. M., Beijaars, A. C., Holtslag, A. A., and Lock, A. P.: Representation of boundary-layer  
385 processes in numerical weather prediction and climate models, *Bound.-Lay. Meteorol.*, 177, 511–  
539, <https://doi.org/10.1007/s10546-020-00530-z>, 2020.
- Emerson, E. W., Hodshire, A. L., Debolt, H. M., Billsback, K. R., Pierce, J. R., McMeeking, G. R., and  
Farmer, D. K.: Revisiting particle dry deposition and its role in radiative effect estimates, *P. Natl.  
Acad. Sci. USA*, 117, 26076–26082, <https://doi.org/10.1073/pnas.2014761117>, 2020.
- 390 Esau, I. N., and Byrkjedal, Ø.: Application of large eddy simulation database to optimization of first order  
closure for neutral and stably stratified boundary layers, *Bound.-Lay. Meteorol.*, 125, 207–225,  
<https://doi.org/10.1007/s10546-007-9213-6>, 2007.
- Foreman, R. J., and Emeis, S.: A Method for Increasing the Turbulent Kinetic Energy in the Mellor–  
Yamada–Janjić Boundary-Layer Parametrization, *Bound.-Lay. Meteorol.*, 145, 329–349,  
395 <https://doi.org/10.1007/s10546-012-9727-4>, 2012.
- Gao, J., Zhu, B., Xiao, H., Kang, H., Pan, C., and Wang, D., and Wang, H.: Effects of black carbon and  
boundary layer interaction on surface ozone in Nanjing, China, *Atmos. Chem. Phys.*, 18, 7081–7094,  
<https://doi.org/10.5194/acp-18-7081-2018>, 2018.
- Gao, M., Han, Z., Tao, Z., Li, J., Kang, J.-E., Huang, K., Dong, X., Zhuang, B., Li, S., Ge, B., Wu, Q.,  
400 Lee, H.-J., Kim, C.-H., Fu, J. S., Wang, T., Chin, M., Li, M., Woo, J.-H., Zhang, Q., Cheng, Y., Wang,  
Z., and Carmichael, G. R.: Air quality and climate change, Topic 3 of the Model Inter-Comparison  
Study for Asia Phase III (MICS-Asia III) – Part 2: aerosol radiative effects and aerosol feedbacks,  
*Atmos. Chem. Phys.*, 20, 1147–1161, <https://doi.org/10.5194/acp-20-1147-2020>, 2020.
- Gao, Z., Liu, H., Li, D., Katul, G. G., and Blanken, P. D.: Enhanced temperature-humidity similarity  
405 caused by entrainment processes with increased wind shear, *J. Geophys. Res.-Atmos.*, 123, 4110–  
4121, <https://doi.org/10.1029/2017JD028195>, 2018.



- Grell, G. A., and Devenyi, D.: A generalized approach to parameterizing convection combining ensemble and data assimilation techniques, *Geophys. Res. Lett.*, 29, 1693, <https://doi.org/10.1029/2002GL015311>, 2002.
- 410 Gu, H., Jin, J., Wu, Y., Ek, M. B., and Subin, Z. M.: Calibration and validation of lake surface temperature simulations with the coupled WRF-lake model, *Clim. Change*, 129, 471–483, <https://doi.org/10.1007/s10584-013-0978-y>, 2015.
- Guo, X., Sun, Y., and Miao, S.: Characterizing urban turbulence under haze pollution: insights into temperature-humidity dissimilarity, *Bound.-Lay. Meteorol.*, 158, 501–510, <https://doi.org/10.1007/s10546-015-0104-y>, 2016.
- 415 Guo, X., Yang, K., Yang, W., Zhao, L., Li, S., and Ding, B.: Representing the heat-to-moisture transport efficiency in stable conditions: an extension of two different approaches, *Asia-Pac. J. Atmos. Sci.*, 56, 603–611, <https://doi.org/10.1007/s13143-019-00155-4>, 2020.
- Huang, Y., and Peng, X.: Improvement of the Mellor–Yamada–Nakanishi–Niino Planetary Boundary-  
420 Layer Scheme Based on Observational Data in China, *Bound.-Lay. Meteorol.*, 162, 171–188, <https://doi.org/10.1007/s10546-016-0187-0>, 2017.
- Iacono, M. J., Delamere, J. S., Mlawer, E. J., Shephard, M. W., Clough, S. A., and Collins, W. D.: Radiative forcing by long-lived greenhouse gases: calculations with the AER radiative transfer models, *J. Geophys. Res.-Atmos.*, 113, D13103. <https://doi.org/10.1029/2008JD009944>, 2008.
- 425 Jia, W., and Zhang, X.: The role of the planetary boundary layer parameterization schemes on the meteorological and aerosol pollution simulations: A review, *Atmos. Res.*, 239, 104890, <https://doi.org/10.1016/j.atmosres.2020.104890>, 2020.
- Jia, W., Zhang, X., Zhang, H., and Ren, Y.: Application of turbulent diffusion term of aerosols in mesoscale model, *Geophys. Res. Lett.*, <https://doi.org/10.1029/2021GL093199>, 2021.
- 430 Jiménez, P. A., Dudhia, J., González–Rouco, J. F., Navarro, J., Montávez, J. P., and García–Bustamante E.: A revised scheme for the WRF surface layer formulation, *Mon. Wea. Rev.*, 140, 898–918, <https://doi.org/10.1175/MWR-D-11-00056.1>, 2012.
- Katul, G. G., Sempreviva, A. M., and Cava, D.: The temperature-humidity covariance in the marine surface layer: a one-dimensional analytical model, *Bound.-Lay. Meteorol.*, 126, 263–278, <https://doi.org/10.1007/s10546-007-9236-z>, 2008.
- 435



- Kays, W. M., Crawford, M. E., and Weigand, B.: Convective heat and mass transfer. McGraw-Hill Higher Education, Boston, 2005.
- Kusaka, H., Kondo, H., Kikegawa, Y., and Kimura, F.: A simple single-layer urban canopy model for atmospheric models: comparison with multi-layer and slab models. *Bound.-Lay. Meteorol.*, 101, 329–358, <https://doi.org/10.1023/a:1019207923078>, 2001.
- 440 LeMone, M. A., Angevine, W. M., Bretherton, C. S., Chen, F., Dudhia, J., Fedorovich, E., Katsaros, K. B., Lenschow, D. H., Mahrt, L., Patton, E. G., Sun, J. L., Tjernström, M., and Weil, J.: 100 Years of progress in boundary layer meteorology, *Meteorol. Mono.*, 59, 9.1–9.85, <https://academic.microsoft.com/paper/2935666247>, 2019.
- 445 Li, D., and Bou-Zeid, E.: Coherent structures and the dissimilarity of turbulent transport of momentum and scalars in the unstable atmospheric surface layer, *Bound.-Lay. Meteorol.*, 140, 243–262, <https://doi.org/10.1007/s10546-011-9613-5>, 2011.
- Li, M., Wang, T., Xie, M., Zhuang, B., Li, S., Han, Y., and Chen, P.: Impacts of aerosol-radiation feedback on local air quality during a severe haze episode in Nanjing megacity, eastern China, *Tellus B: Chem. Phys. Meteorol.*, 69, 1339548, <https://doi.org/10.1080/16000889.2017.1339548>, 2017.
- 450 Li, X., Gao, C. Y., Gao, Z., and Zhang, X.: Atmospheric boundary layer turbulence structure for severe foggy haze episodes in north China in December 2016, *Environ. Pollut.*, 264, 114726, <https://doi.org/10.1016/j.envpol.2020.114726>, 2020.
- Li, Y., Gao, Z., Lenschow, D. H., and Chen, F.: An improved approach for parameterizing surface-layer turbulent transfer coefficients in numerical models, *Bound.-Lay. Meteorol.*, 137, 153–165, <https://doi.org/10.1007/s10546-010-9523-y>, 2010.
- Lin, J., Youn, D., Liang, X., and Wuebbles, D. J.: Global model simulation of summertime U.S. ozone diurnal cycle and its sensitivity to PBL mixing, spatial resolution, and emissions, *Atmos. Environ.*, 42, 8470–8483, <https://doi.org/10.1016/j.atmosenv.2008.08.012>, 2008.
- 460 Liu, C., Huang, J. Hu, X.-M., Hu, C., Wang, Y., Fang, X., Luo, L., Xiao, H., and Xiao, H.: Evaluation of WRF-Chem simulations on vertical profiles of PM<sub>2.5</sub> with UAV observations during a haze pollution event, *Atmos. Environ.*, 252, 118332, <https://doi.org/10.1016/j.atmosenv.2021.118332>, 2021.
- Liu, M., Lin, J., Wang, Y., Sun, Y., Zheng, B., and Shao, J., Chen, L., Zheng, Y., Chen, J., Fu, T.-M., Yan, Y., Zhang, Q., and Wu, Z.: Spatiotemporal variability of NO<sub>2</sub> and PM<sub>2.5</sub> over Eastern China:



- 465        observational and model analyses with a novel statistical method, *Atmos. Chem. Phys.*, 18, 12933–  
12952, <https://doi.org/10.5194/acp-18-12933-2018>, 2018.
- Liu, M., and Carroll, J. J.: A high-resolution air pollution model suitable for dispersion studies in complex  
terrain, *Mon. Wea. Rev.*, 124, 2396–2409, [https://doi.org/10.1175/1520-0493\(1996\)124<2396:ahrapm>2.0.co;2](https://doi.org/10.1175/1520-0493(1996)124<2396:ahrapm>2.0.co;2), 1996.
- 470    Liu, Y., Liu, H., Wang, L. The vertical distribution characteristics of integral turbulence statistics in the  
atmospheric boundary layer over an urban area in Beijing. *Science China Earth Sciences*, 60, 1533–  
1545, <https://doi.org/10.1007/s11430-016-9050-5>, 2017
- Louis, J.: A parametric model of vertical eddy fluxes in the atmosphere, *Bound.-Lay. Meteorol.*, 17, 187–  
202, <https://doi.org/10.1007/BF00117978>, 1979.
- 475    Miao, Y., Che, H., Zhang, X., and Liu, S.: Relationship between summertime concurring PM<sub>2.5</sub> and O<sub>3</sub>  
pollution and boundary layer height differs between Beijing and Shanghai, China, *Environ. Pollut.*,  
268, 115775, <https://doi.org/10.1016/j.envpol.2020.115775>, 2021.
- Miao, Y., Liu, S., Guo, J., Huang, S., Yan, Y., and Lou, M.: Unraveling the relationships between  
boundary layer height and PM<sub>2.5</sub> pollution in China based on four-year radiosonde measurements,  
480    *Environ. Pollut.*, 243, 1186–1195, <https://doi.org/10.1016/j.envpol.2018.09.070>, 2018.
- Moriwaki, R., and Kanda, M.: Local and global similarity in turbulent transfer of heat, water vapour, and  
CO<sub>2</sub> in the dynamic convective sublayer over a suburban area, *Bound.-Lay. Meteorol.*, 120, 163–  
179, <https://doi.org/10.1007/s10546-005-9034-4>, 2006.
- Morrison, H., Thompson, G., and Tatarskii, V.: Impact of Cloud Microphysics on the Development of  
485    Trailing Stratiform Precipitation in a Simulated Squall Line: Comparison of One- and Two-  
Moment Schemes, *Mon. Wea. Rev.*, 137, 991–1007, <https://doi.org/10.1175/2008MWR2556.1>,  
2009.
- Pleim, J. E.: A combined local and nonlocal closure model for the atmospheric boundary layer. Part I:  
model description and testing, *J. Appl. Meteorol. Climatol.*, 46, 1383–1395,  
490    <https://doi.org/10.1175/JAM2539.1>, 2017.
- Pleim, J. E., Gilliam, R., Appel, W., and Ran, L.: Recent advances in modeling of the atmospheric  
boundary layer and land surface in the coupled WRF-CMAQ model, *Air Pollution Modeling and its  
Application XXIV*, 391–396, [https://doi.org/10.1007/978-3-319-24478-5\\_64](https://doi.org/10.1007/978-3-319-24478-5_64), 2016.



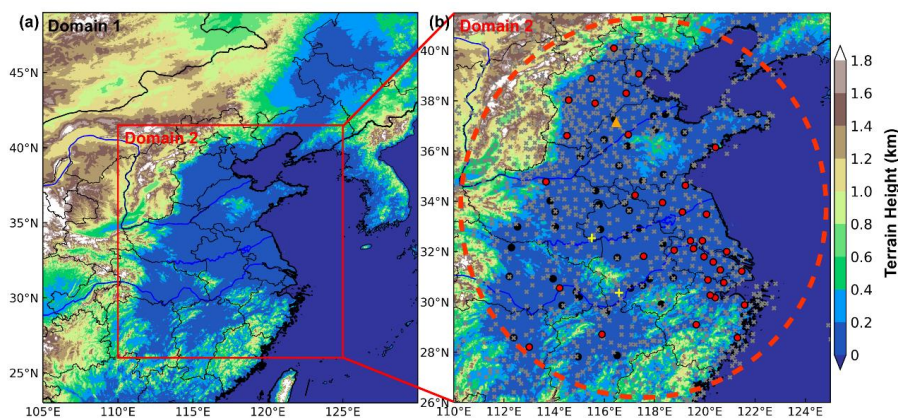
- Ren, Y., Zhang, H., Wei, W., Cai, X., and Song, Y.: Determining the fluctuation of PM<sub>2.5</sub> mass  
495 concentration and its applicability to Monin–Obukhov similarity, *Sci. Total Environ.*, 710, 136398,  
<https://doi.org/10.1016/j.scitotenv.2019.136398>, 2020.
- Ren, Y., Zhang, H., Zhang, X., Li, Q., Cai, X., Song, Y., Kang, L., and Zhu, T.: Temporal and spatial  
characteristics of turbulent transfer and diffusion coefficient of PM<sub>2.5</sub>, *Sci. Total Environ.*, 782,  
146804, <https://doi.org/10.1016/j.scitotenv.2021.146804>, 2021.
- 500 Ren, Y., Zheng, S., Wei, W., Wu, B., Zhang, H., Cai, X., and Song, Y.: Characteristics of the turbulent  
transfer during the heavy haze in winter 2016/17 in Beijing, *J. Meteor. Res.*, 32, 69–80,  
<https://doi.org/10.1007/s13351-018-7072-3>, 2018.
- Savijärvi, H., and Kauhanen, J.: High resolution numerical simulations of temporal and vertical  
variability in the stable wintertime boreal boundary layer: a case study, *Theor. Appl. Climaol.*, 70,  
505 97–103, <https://doi.org/10.1007/s007040170008>, 2002.
- Schell, B., Ackermann, I. J., and Hass, H.: Modeling the formation of secondary organic aerosol within  
a comprehensive air quality model system, *J. Geophys. Res.*, 106, 28275–28293,  
<https://doi.org/10.1029/2001JD000384>, 2001.
- Seinfeld, J. H., Bretherton, C., Carslaw, K. S., Coe, H., DeMott, P. J., Dunlea, E. J., Feingold, G., Ghan,  
510 S., Guenther, A. B., Kahn, R., Kraucunas, I., Kreidenweis, S. M., Molina, M. J., Nenes, A., Penner,  
J. E., Prather, K. A., Ramanathan, V., Ramaswamy, V., Rasch, P. J., Ravishankara, A. R., Rosenfeld,  
D., Stephens, G., and Wood, R.: Improving our fundamental understanding of the role of aerosol-  
cloud interactions in the climate system, *P. Natl. Acad. Sci. USA*, 113, 5781–5790.  
<https://doi.org/10.1073/pnas.1514043113>, 2016.
- 515 Shao, J., Chen, Q., Wang, Y., Lu, X., He, P., Sun, Y., Shah, V., Martin, R. V., Philip, S., Song, S., Zhao,  
Y., Xie, Z., Zhang, L., and Alexander, B.: Heterogeneous sulfate aerosol formation mechanisms  
during wintertime Chinese haze events: air quality model assessment using observations of sulfate  
oxygen isotopes in Beijing, *Atmos. Chem. Phys.*, 19, 6107–6123. [https://doi.org/10.5194/acp-19-  
6107-2019](https://doi.org/10.5194/acp-19-6107-2019), 2019.
- 520 Smedman, A.-S., Högström, U., Hunt, J. C. R., and Sahlée, E.: Heat/mass transfer in the slightly unstable  
atmospheric surface layer, *Q. J. R. Meteorol. Soc.* 133, 37–51. <https://doi.org/10.1002/qj.7>, 2007.
- Stull, R. B.: An introduction to boundary layer meteorology, *Atmospheric Sciences Library*, 6, 206–210,  
1988.



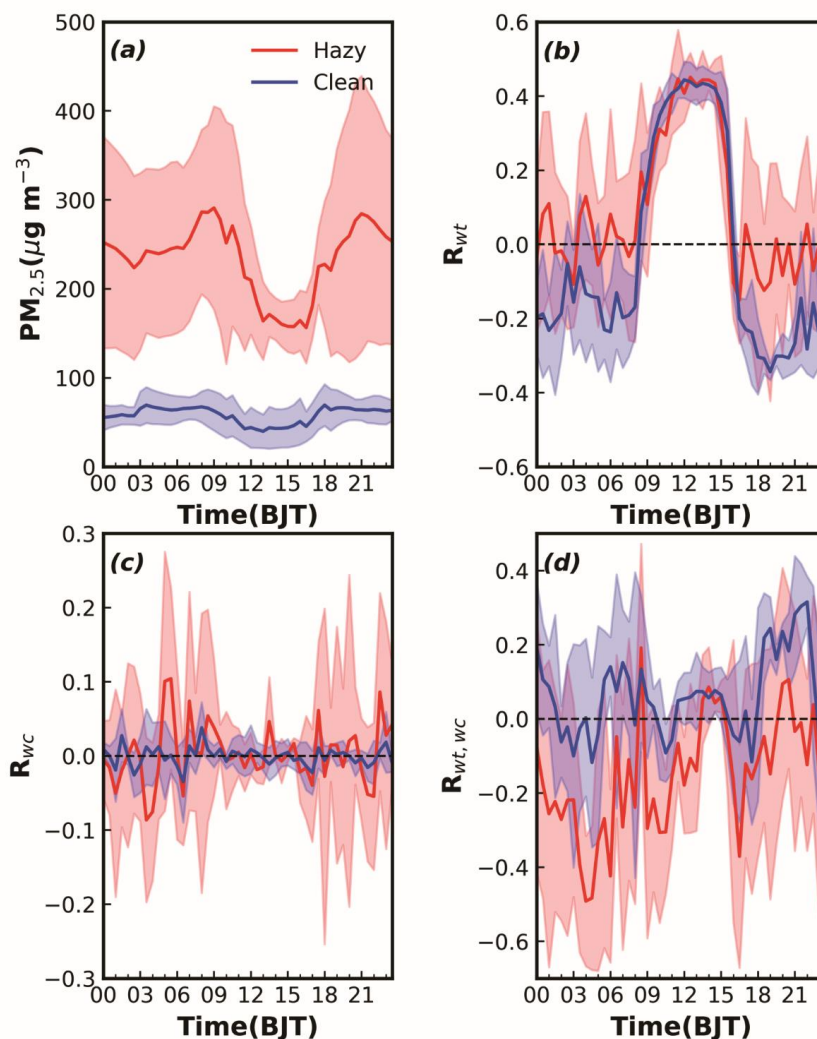
- Subin, Z. M., Riley, W. J., and Mironov, D.: An improved lake model for climate simulations: Model  
525 structure, evaluation, and sensitivity analyses in CESM1, *J. Adv. Model. Earth Syst.*, 4, M02001,  
<https://doi.org/10.1029/2011MS000072>, 2012.
- Sušelj, K., and Sood, A.: Improving the Mellor–Yamada–Janjić Parameterization for wind conditions in  
the marine planetary boundary layer, *Bound.-Lay. Meteorol.*, 136, 301–324.  
<https://doi.org/10.1007/s10546-010-9502-3>, 2010.
- 530 van de Boer, A., Moene, A. F., Graf, A., Schüttemeyer, D., and Simmer, C.: Detection of entrainment  
influences on surface-layer measurements and extension of Monin–Obukhov similarity theory,  
*Bound.-Lay. Meteorol.*, 152:19–44, <https://doi.org/10.1007/s10546-014-9920-8>, 2014.
- Wang, L., Li, D., Gao, Z., Sun, T., Guo, X., and Bou-Zeid, E.: Turbulent transport of momentum and  
scalars above an urban canopy, *Bound.-Lay. Meteorol.*, 150:485–511,  
535 <https://doi.org/10.1007/s10546-013-9877-z>, 2014.
- Wang, H., Peng, Y., Zhang, X., Liu, H., Zhang, M., Che, H., Cheng, Y., and Zheng, Y.: Contributions to  
the explosive growth of PM<sub>2.5</sub> mass due to aerosol–radiation feedback and decrease in turbulent  
diffusion during a red alert heavy haze in Beijing–Tianjin–Hebei, China, *Atmos. Chem. Phys.* 18,  
17717–17733. <https://doi.org/10.5194/acp-18-17717-2018>, 2018.
- 540 Wu, J., Bei, N., Hu, B., Liu, S., Zhou, M., Wang, Q., Li, X., Liu, L., Feng, T., Liu, Z., Wang, Y., Cao, J.,  
Tie, X., Wang J., Molina, L. T., and Li, G.: Aerosol–radiation feedback deteriorates the wintertime  
haze in the North China Plain, *Atmos. Chem. Phys.*, 19, 8703–8719, <https://doi.org/10.5194/acp-19-8703-2019>, 2019.
- Yang, Y., Zheng, X., Gao, Z., Wang, H., Wang, T., Li, Y., Lau, G. N. C., and Yim, S. H. L.: Long-term  
545 trends of persistent synoptic circulation events in planetary boundary layer and their relationships  
with haze pollution in winter half year over eastern China, *J. Geophys. Res.-Atmos.*, 123, 10,991–  
11,007. <https://doi.org/10.1029/2018JD028982>, 2018.
- Yuan, R., Zhang, X., Liu, H., Gui, Y., Shao, B., and Tao, X., Wang, Y., Zhong, J., Li, Y., and Gao, Z.:  
550 Aerosol vertical mass flux measurements during heavy aerosol pollution episodes at a rural site  
and an urban site in the Beijing area of the North China Plain, *Atmos. Chem. Phys.*, 19, 12857–  
12874, <https://doi.org/10.5194/acp-19-12857-2019>, 2019.



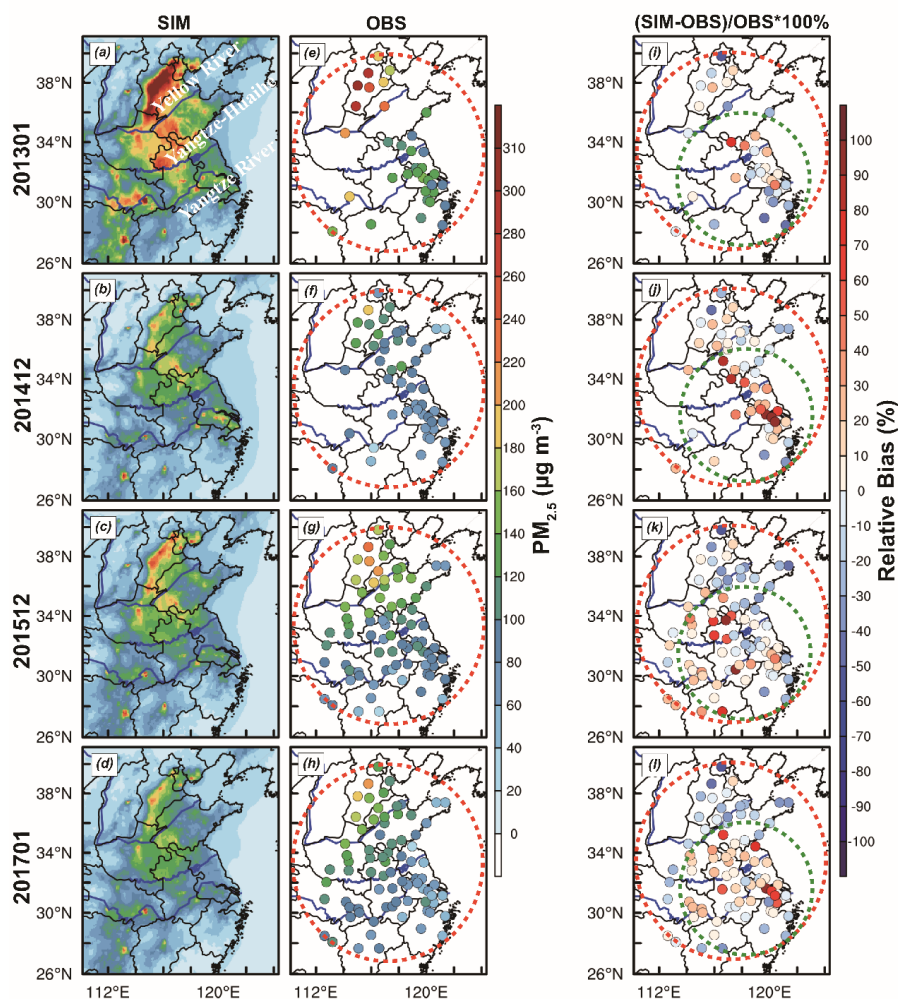
- Zhang, H., Zhang, X., Li, Q., Cai, X., Fan, S., Song, Y., Hu, F., Che, H., Quan, J., Kang, L., and Zhu, T.:  
Research progress on estimation of the atmospheric boundary layer height, *J. Meteor. Res.*, 34, 482–  
498, <https://doi.org/10.1007/s13351-020-9910-3>, 2020.
- 555 Zhang, Q., Zheng, Y., Tong, D., Shao, M., Wang, S., Zhang, Y., Xu, X., Wang, J., He, H., Liu, W., Ding,  
Y., Lei, Y., Li, J., Wang, Z., Zhang, X., Wang, Y., Cheng, J., Liu, Y., Shi, Q., Yan, L., Geng, G., Hong,  
C., Li, M., Liu, F., Zheng, B., Cao, J., Ding, A., Gao, J., Fu, Q., Huo, J., Liu, B., Liu, Z., Yang, F.,  
He, K., and Hao, J.: Drivers of improved PM<sub>2.5</sub> air quality in China from 2013 to 2017, *P. Natl. Acad.  
Sci. USA*, 116, 24463–24469. <https://doi.org/10.1073/pnas.1907956116>, 2019.
- 560 Zhang, X., Xu, X., Ding, Y., Liu, Y., Zhang, H., Wang, Y., and Zhong, J.: The impact of meteorological  
changes from 2013 to 2017 on PM<sub>2.5</sub> mass reduction in key regions in China, *Sci. China Earth Sci.*,  
62, 1–18. <https://doi.org/10.1007/s11430-019-9343-3>, 2019.
- Zhong, J., Zhang, X., Wang, Y., Wang, J., Sheng, X., Zhang, H., Wang, T., Xie, Z., Liu C., Zhang, H.,  
Zhao, T., Sun, J., Fan, S., Gao, Z., Li, Y., and Wang, L.: The two-way feedback mechanism between  
565 unfavorable meteorological conditions and cumulative aerosol pollution in various haze regions of  
China, *Atmos. Chem. Phys.*, 19, 3287–3306, <https://doi.org/10.5194/acp-19-3287-2019>, 2019.



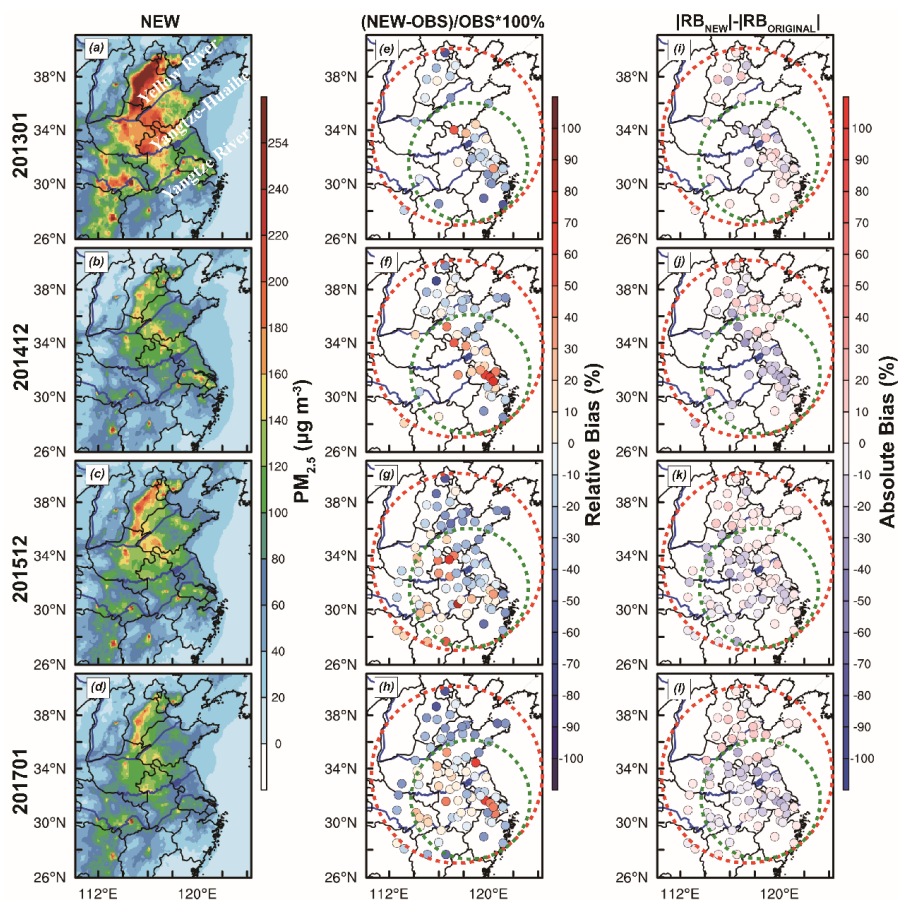
570 **Figure 1. (a) Map of terrain height in the two nested model domains. (b) The locations of surface meteorological stations, air quality monitoring stations and sounding stations are marked by the gray crosses, red(black) dots and yellow pluses, respectively. The turbulence data site is denoted by the orange triangle. The red dashed circle indicates the areas of our primary concern.**



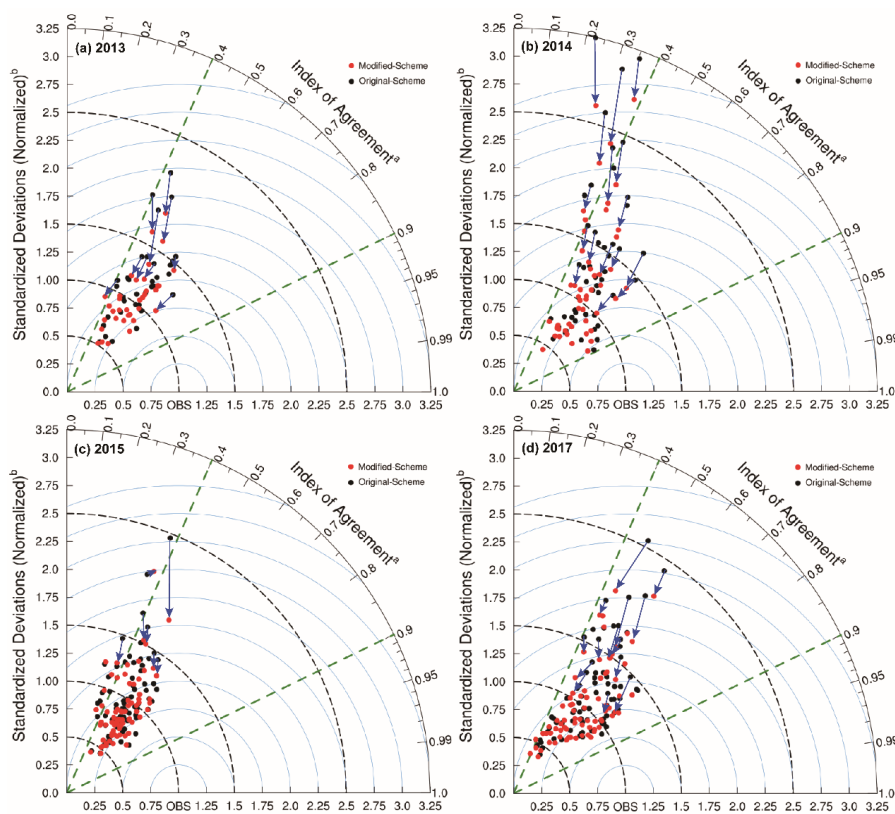
575 **Figure 2.** Diurnal variations of (a) PM<sub>2.5</sub> concentration, (b) transport efficient of heat flux ( $R_{wt}$ ), (c) transport efficient for fine particles flux ( $R_{wc}$ ) and (d) correlations of heat and fine particles fluxes ( $R_{wt,wc}$ ). The red (blue) line represents the heavy (cleaning) pollution episodes, and the shaded area indicates the average value  $\pm$  standard deviation.



580 **Figure 3.** The average value of (a-d) simulated and (e-h) observed  $\text{PM}_{2.5}$  concentration ( $\mu\text{g m}^{-3}$ ) at night, (i-l) the relative bias (RB, %) between simulation and observation, and the calculation formula of relative bias is  $\text{RB} = \frac{(\overline{X}_{\text{sim}} - \overline{X}_{\text{obs}})}{\overline{X}_{\text{obs}}} \times 100\%$ , where  $\overline{X}_{\text{sim}}$  and  $\overline{X}_{\text{obs}}$  represent the average value of simulation and observation, respectively. The locations of three rivers (i.e., Yellow River, Yangtze-Huaihe and Yangtze River) are marked by blue lines.



585 **Figure 4.** The average value of (a-d) simulated  $PM_{2.5}$  concentration ( $\mu\text{g m}^{-3}$ ) by new schemes, (e-h) the relative bias (RB, %) of  $PM_{2.5}$  concentration between simulation of new scheme and observation, (i-l) the absolute bias (AB, %) between new and original schemes, and the calculation formula of absolute bias is  $AB = |RB_{\text{new}}| - |RB_{\text{original}}|$ , where  $|RB_{\text{new}}|$  and  $|RB_{\text{original}}|$  represent the relative bias of new and original schemes, respectively.



590

Figure 5. Taylor diagram of simulation by original scheme and modified scheme. XY axes and arc represent the normalized standardized deviations (NSTD,

$$\text{NSTD} = \frac{\sqrt{\frac{1}{N-1} \sum_{i=1}^n (X_{\text{sim},i} - \overline{X}_{\text{sim}})^2}}{\sqrt{\frac{1}{N-1} \sum_{i=1}^n (X_{\text{obs},i} - \overline{X}_{\text{obs}})^2}}, \quad \overline{X}_{\text{sim}} \quad \text{and} \quad \overline{X}_{\text{obs}}$$

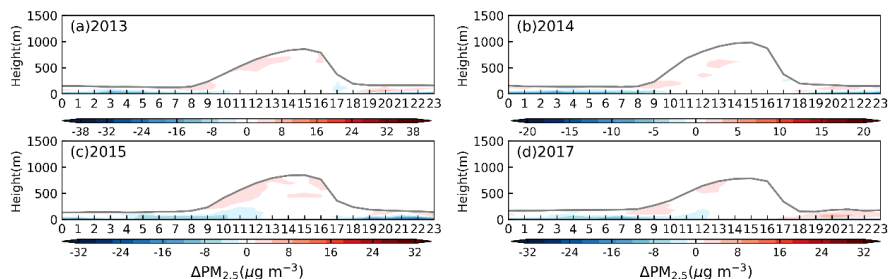
simulation and observation, respectively) and index of agreement (IOA,

$$\text{IOA} = 1 - \frac{\left[ \sum_{i=1}^n |X_{\text{sim},i} - X_{\text{obs},i}|^2 \right]}{\left[ \sum_{i=1}^n (|X_{\text{sim},i} - \overline{X}_{\text{obs}}| + |X_{\text{obs},i} - \overline{X}_{\text{obs}}|)^2 \right]}, \quad X_{\text{sim},i} \quad \text{and} \quad X_{\text{obs},i}$$

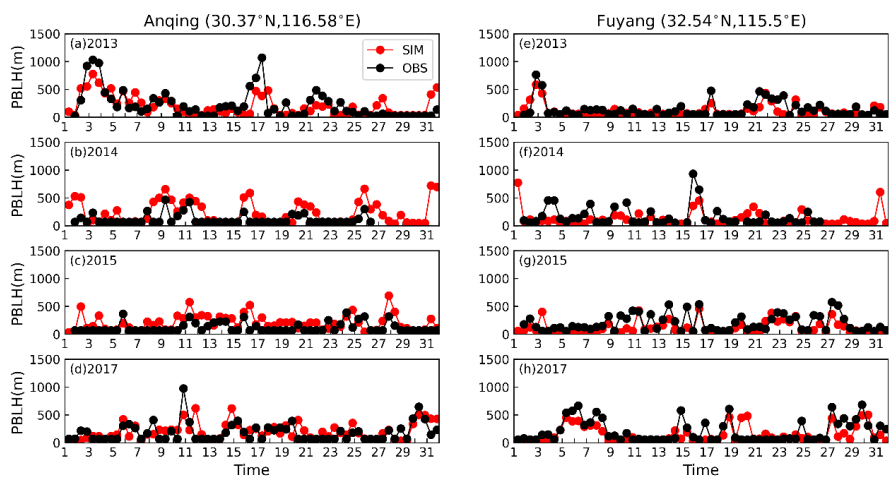
595

simulated and observed, respectively.  $i$  refers to time and  $n$  is the total number of time series, respectively. All cities (a total of 35 cities in 2013 and 78 cities in 2014, 2015 and 2017) are shown through dots, and black (red) represents original (new) scheme. The root mean square (RMS) is denoted by blue dashed line and the arrow indicates the change of the new scheme compared to the original scheme at the same station.

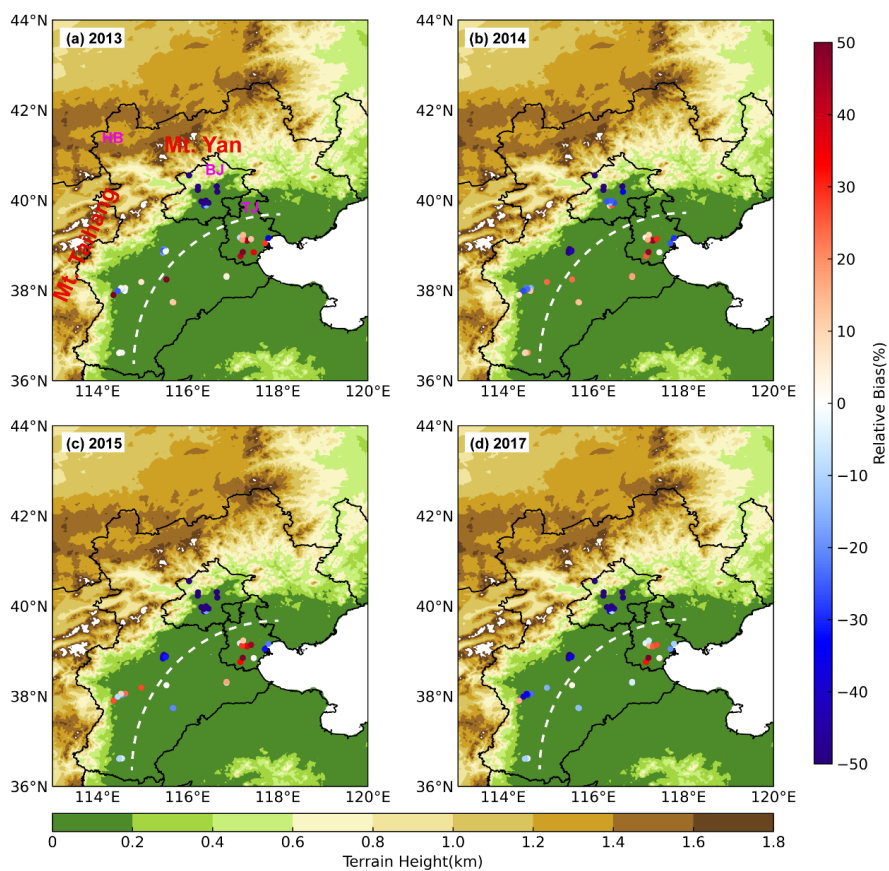
600



605 **Figure 6.** Time-height cross sections for the difference of  $PM_{2.5}$  concentration between original and new schemes (i.e., the new scheme minus the original scheme) within the PBL. The gray line indicates the PBLH.



**Figure 7.** Time series of the observed (black) and simulated (red) PBLH at 0800 and 2000 (BJT) in the (a-d) Anqing and (e-h) Fuyang from 2013 to 2017.



610 **Figure 8.** The relative bias (%) between simulation and observation at all environment  
615 **monitoring stations and terrain height in Beijing-Tianjin-Hebei in (a) 2013, (b) 2014, (c) 2015**  
**and (d) 2017. Taihang mountain and Yan mountain are indicated by red text, Beijing (BJ), Tianjin**  
**(TJ) and Hebei (HB) are represented by purple abbreviation and the dividing line between**  
**overestimated and underestimated areas is indicated by a white dashed line.**